Modeling the optical dielectric function of the alloy system $Al_xGa_{1-x}As$

Charles C. Kim,* J. W. Garland, and P. M. Raccah
Department of Physics, University of Illinois at Chicago, P.O. Box 4348, Chicago, Illinois 60680
(Received 27 August 1992)

In a previous paper, the authors proposed a model for the optical dielectric function of zinc-blende semiconductors. It was found to be more generally valid than previous models. In this paper, it is used to obtain an analytic expression for the dielectric function of the alloy series $Al_xGa_{1-x}As$ as a function of ω and x, which is compared with spectroscopic ellipsometry data between 1.5 and 6.0 eV. The model enables us to determine accurately the critical point energies and linewidths of $Al_xGa_{1-x}As$ as a function of x. Also, it leads us to model the optical dielectric function of these alloys better than any previous model in that (1) it covers the entire photon energy range between 1.5 and 6.0 eV as well as the entire alloy composition range between 0.0 and 1.0, (2) it calculates the optical properties of $Al_xGa_{1-x}As$ as a function of ω and x with the highest accuracy, and (3) it allows one to accurately calculate the values of the refractive indices below 1.5 eV as a function of ω and x.

I. INTRODUCTION

In a previous paper the authors proposed a model[1] for the optical dielectric function of GaAs and successfully applied it to fit the spectral data of the dielectric function of GaAs. It was found to be more generally valid than previous models. In this paper we use this model to obtain a closed analytic formula for the optical dielectric function of the alloy series as a function of x. This is possible because the band structure of $Al_xGa_{1-x}As$ does not vary much as x changes, so that the joint density of states $J(E)$ has an analytic structure which is independent of x within a reasonable approximation.

The measured optical properties of semiconductor materials, such as the complex dielectric function,[2] $\epsilon(\omega) \equiv \epsilon_1(\omega) + i\epsilon_2(\omega)$, the complex refractive index, $N(\omega) \equiv n(\omega) + ik(\omega)$, the reflectance[3] $R(\omega)$, and the absorption coefficient $\alpha(\omega)$, have proven very useful in describing the electronic structure of these materials. An accurate knowledge of their values is essential in a number of applications, such as in the real-time monitoring and control of crystal growth and/or etching with single-wavelength and spectroscopic ellipsometry, in designing optoelectronic devices and in analyzing[4] the spectral data of multilayer systems. Among these properties, $\epsilon(\omega)$ is the most fundamental from a theoretical point of view and is most closely related to the electronic band structure. In particular, in the absence of line broadening, $\epsilon_2(\omega)$ is approximately proportional[5] to $J(E)$. All other optical properties of any semiconductor material are easily expressed as simple functions of $\epsilon(\omega)$.

Recently, Aspnes *et al.*[6] have measured the optical properties of $Al_xGa_{1-x}As$ alloys at room temperature by spectroscopic ellipsometry (SE). They reported the spectral data of the dielectric function of $Al_xGa_{1-x}As$, $L(\omega_j, x_k) \equiv L_1(\omega_j, x_k) + iL_2(\omega_j, x_k)$, over the photon-energy range from 1.5 to 6.0 eV in steps of about 18 meV, with x_k varying from 0.0 to 0.9 in steps of 0.1. Garriga *et al.*[7] have presented SE data of the dielectric function of AlAs, $L(\omega_j, 1)$, at room temperature from 1.66 to 5.6 eV in steps of 10 meV. Fitting the data of Refs. 6 and 7 with our new model, we obtain its analytical expression $\epsilon(\omega, x)$ and predict $n(\omega, x)$ below the available spectral data down to optical-phonon frequencies for $Al_xGa_{1-x}As$.

A very important recent application of single-wavelength and spectroscopic ellipsometry is the real-time monitoring and control of crystal growth and etching. Recent work in this area[8,9] points out that proper methods of interpolation for $\epsilon(\omega)$ are essential to obtain accurate alloy content and/or temperature during molecular-beam epitaxy or metal-organic chemical-vapor deposition growth or ion-beam and/or reactive-ion etching. This paper demonstrates a substantially more accurate method of interpolation in x for $\epsilon(\omega, x)$ than has been previously available. We plan to apply the same method to calculate $\epsilon(\omega, T)$ in a later paper.

The alloy system $Al_xGa_{1-x}As$ has been widely used for many high-speed electronic and optoelectronic devices. These alloys are essentially lattice matched with a mismatch of less than 0.15% and are valence-bond matched over the entire composition range. This has made it possible to grow artificial structures with excellent interface properties, including heterostructures,[10] quantum wells,[11] superlattices,[12] and resonant tunneling structures. In developing optoelectronic devices which utilize $Al_xGa_{1-x}As$ alloys, the optical properties of these alloys must be well known. In the construction of solid-state lasers and waveguiding devices which utilize these materials, the interplay between the physical dimensions of the device and the refractive indices requires the refractive indices to be known as a function of ω and x as precisely as possible. Also it often is essential to fit or simulate the spectral data of quantum wells or superlattices made of $Al_xGa_{1-x}As$ alloys which consist of more

than two layers. However, doing so is extremely difficult without knowing the dielectric function of each layer as a function of ω and x. Furthermore, the resultant analysis largely depends[13] on the accuracy of the calculated dielectric function for each layer. Thus, it is important to have as accurate as possible a model for the optical dielectric function of $Al_xGa_{1-x}As$ alloys.

There have been various models for $\epsilon(\omega, x)$ for $Al_xGa_{1-x}As$ and other tetrahedrally bonded semiconductor alloy series. Aspnes[6] suggested that one can use either the interpolation scheme or the harmonic oscillator (HO) model to calculate $\epsilon(\omega, x)$ from his discrete spectral data points, $L(\omega_j, x_k)$. The HO model has been used[14,15] for the analysis of multilayer systems. This model was improved by Terry,[13] who demonstrated the significance of its improvement in the analysis of multilayer systems. Snyder *et al.*[16] used an interpolation method to calculate $\epsilon(\omega, x)$ and demonstrated that their method gives better results around the band edge than does the effective-medium approximation. Recently, Adachi developed a new model[17] for the dielectric function of semiconductor materials and used that model to calculate $\epsilon(\omega, x)$ for $Al_xGa_{1-x}As$.[18] Later, Jenkins[19] substantially improved the model of Adachi and used the improved model to recalculate $\epsilon(\omega, x)$.

Recently, we have developed a new model[1] for the dielectric function of zinc-blende semiconductors and have shown it to be more generally valid than any of the previous models. Thus, this model is expected to produce a better and more physically significant fit to the spectral data of $Al_xGa_{1-x}As$ than that given by any previous model. This model enables us to determine accurately the critical point energies and linewidths of $Al_xGa_{1-x}As$. Consequently, it enables us to calculate the optical properties of $Al_xGa_{1-x}As$ better than any previous models in that (1) it covers the entire photon-energy range between 1.5 and 6.0 eV as well as the entire alloy composition range between 0.0 and 1.0, (2) it calculates the optical properties with the highest accuracy, and (3) it allows one to calculate easily the values of the refractive index below 1.5 eV as a function of ω and x.

This paper is organized as follows. In Sec. II we briefly explain how to model $L(\omega_j, x_k)$. In Sec. III our model is applied to $L(\omega_j, 1)$, using a simpler approximation than that used to fit $L(\omega_j, 0)$ in the previous paper. In Sec. IV we determine the critical-point (CP) energies, E_i, and line widths, Γ_i, as a function of x. In Sec. V we show how to calculate $\epsilon(\omega, x)$, using the values for the $E_i(x)$ and $\Gamma_i(x)$ determined in Sec. IV. Our results are compared with those obtained using other models.

II. A MODEL FOR THE DIELECTRIC FUNCTION OF $Al_xGa_{1-x}As$

The optical dielectric function[1] of solid-state materials with Lorentzian line broadening is given by the equation

$$\epsilon(\omega) = 1 - \frac{8\pi\hbar^2 e^2}{m^2} \sum_{c,v} \int \frac{W_{cv}(E)dE}{E^2} \left[\frac{1}{\hbar\omega - E + i\Gamma} - \frac{1}{\hbar\omega + E + i\Gamma} \right], \tag{1}$$

where

$$W_{cv}(E) = P_{cv}(E)^2 J_{cv}(E),$$

c and v stand for the conduction and valence bands, respectively, $E \equiv E_{cv}(\mathbf{k})$ is the energy difference between a pair of bands in $\mathbf{k}$ space, $J_{cv}(E)$ is the joint density of states between a pair of bands, and $P_{cv}(E)$ is the weighted-average matrix element of the momentum operator. Similarly, the optical dielectric function of solid state materials with Gaussian broadening is given by the equation

$$\epsilon(\omega) = 1 + i\frac{8\pi\hbar^2 e^2}{m^2} \sum_{c,v} \int \frac{W_{cv}(E)dE}{E^2} \left[\int_0^\infty ds\, e^{i(\hbar\omega - E + 2i\sigma^2 s)s} - \int_0^\infty ds\, e^{i(\hbar\omega + E + 2i\sigma^2 s)s} \right], \tag{2}$$

where σ is the root-mean-square scattering t matrix. Our model is based on these two equations. It is developed in two steps. The first step is to find a simple functional representation for $W_{cv}(E)$. This representation must fully satisfy the CP behavior of $W_{cv}(E)$ with no artificial cutoffs and it must be capable of accurately mimicking $W_{cv}(E)$ for $Al_xGa_{1-x}As$ for any x value. The second step is to analytically perform the integrals in Eqs. (1) and (2), even if only approximately for the case of Eq. (2).

Let us consider how to construct $W_{cv}(E)$ for $Al_xGa_{1-x}As$. Because $P_{cv}(E)$ is a slowly varying function of E with no singularities, we need only to consider the analytic structure of $J_{cv}(E)$. In developing the analytical form of $J_{cv}(E)$ for the entire $Al_xGa_{1-x}As$ alloy series, we need to ask if its analytic form changes at any composition. The answer is yes, but not in an important way for the purposes of this paper. The crystal structure does not change, but the band structure does change from a direct-band-gap structure to an indirect-band-gap structure around $x = 0.35$. However, because of their very small matrix elements, the indirect transitions contribute only negligibly to $\epsilon(\omega)$, except for the calculation of absorptivity below the direct band gap, with which we are not concerned in this paper. Also, from observing the derivative spectra of $Al_xGa_{1-x}As$, we

find that the number of major critical-point structures is independent of x. From band-structure calculations for GaAs (Ref. 20) and for AlAs,[21] the critical-point types remain the same. Thus, we conclude that the analytical form of $J_{cv}(E)$ needed in our model can be taken to be independent of x, so that we can use the analytic form used for GaAs in the previous paper.

We summarize our model for $W_{cv}(E)$ for GaAs. Only seven critical points are clearly evident in the room-temperature data which we fit. Therefore, in order to reduce the number of parameters in the model, we include only the seven critical points $E_0(\Gamma)$, $E_0(\Gamma)+\Delta_0(\Gamma)$, $E_1(\Lambda)$, $E_1(\Lambda)+\Delta_1(\Lambda)$, $E_0'(\Delta)$, $E_2(X)$, and $E_2(\Sigma)$ in order of increasing energy up to 6 eV. Except for $E_0(\Gamma)$ and $E_0(\Gamma)+\Delta_0(\Gamma)$, each of these critical points is allowed to contain a two-dimensional (2D) contribution. The resultant discontinuities divide the range of interest, from 1.0 to 6.0 eV, into six segments, which are designated by I, II, III, IV, V, and VI in order of increasing energy. Knowing that $E_0(\Gamma)$ and $E_0(\Gamma)+\Delta_0(\Gamma)$ have three-dimensional (3D) M_0 critical points, that the $E_1(\Lambda)$, $E_1(\Lambda)+\Delta_1(\Lambda)$, $E_0'(\Delta)$, and $E_2(X)$ critical points have 3D M_1 contributions and that $E_2(\Sigma)$ CP has a 3D M_2 contribution, one can determine the analytical form of $W_{cv}(E)$ in each segment ν. The resultant analytical forms can be written as follows:

$$W_{\rm I}(E)+W_{\rm I'}(E)=\sqrt{E-E_0}\,[p_{\rm I}(E)+q_{\rm I}(E)\sqrt{E_1-E}]+p_{\rm I'}(E)\sqrt{E-(E_0+\Delta_0)}, \tag{3}$$

$$W_{\rm II}(E)=p_{\rm II}(E)+q_{\rm II}(E)\sqrt{(E_1+\Delta_1)-E}, \tag{4}$$

$$W_{\rm III}(E)=p_{\rm III}(E)+q_{\rm III}(E)\sqrt{E_0'-E}, \tag{5}$$

$$W_{\rm IV}(E)=p_{\rm IV}(E)+q_{\rm IV}(E)\sqrt{E_2(X)-E}, \tag{6}$$

$$W_{\rm V}(E)=p_{\rm V}(E), \tag{7}$$

and

$$W_{\rm VI}(E)=p_{\rm VI}(E)+q_{\rm VI}(E)\sqrt{E-E_2(\Sigma)}, \tag{8}$$

where $p_\nu(E)=\sum_n p_{n,\nu}E^n$ and $q_\nu(E)=\sum_n q_{n,\nu}E^n$ for ν =I,I',II,III,IV,V,VI are low-order polynomials. The contribution of the $E_0(\Gamma)+\Delta_0(\Gamma)$ CP is included in the segment I as $W_{\rm I'}(E)$ without introducing any discontinuity. Summing over all of these contributions leads to the final analytical form for $W(E)=\sum_\nu W_\nu(E)$.

For the case of Lorentzian line broadening, the substitution of $W(E)$ into Eq. (1) leads to the equation

$$\epsilon(\omega)=1-\frac{8\pi\hbar^2e^2}{m^2}\sum_n\,[\,(p_nH_n+q_nF_n)_{\rm I}+(p_nH_n)_{\rm I'}+(p_nG_n+q_nK_n)_{\rm II}+(p_nG_n+q_nK_n)_{\rm III}+(p_nG_n+q_nK_n)_{\rm IV}+(p_nG_n)_{\rm V}+(p_nG_n+q_nH_n)_{\rm VI}]+\sum_n b_n(\hbar\omega)^n, \tag{9}$$

where H_n, F_n, G_n, and K_n are functions of $\hbar\omega$ defined in Appendix A of the previous paper,[1] and where the last term gives the contribution to $\epsilon_1(\omega)$ from critical points above 6 eV. The case of Gaussian line broadening is not as simple because the integral in Eq. (2) cannot be performed analytically. However, the substitution of the quantity

$$D_i=\Gamma_i\,\exp\left[-\alpha_i\left(\frac{\hbar\omega-E_i}{\Gamma_i}\right)^2\right] \tag{10}$$

for Γ_i in H_n, F_n, G_n, and K_n leads to analytic functions which accurately mimic the numerical results for the Gaussian case, for appropriate values of α_i. The value of α_i which most closely mimics the exact results of Gaussian broadening is not exactly the same for the four functions H_n, F_n, G_n, and K_n and depends slightly on the value of n, but is approximately 0.2 in all cases.

Equation (9) is easily extended to apply to the alloy series $Al_xGa_{1-x}As$. Only the values of the parameters E_i, Γ_i, $p_{n,\nu}$, and $q_{n,\nu}$ change from one alloy to another. Thus, Eq. (9) can be made to apply to all $Al_xGa_{1-x}As$ alloys by replacing each of these parameters by a function of x, which leads to the result

$$\epsilon(\omega,x)=1-\frac{8\pi\hbar^2e^2}{m^2}\sum_n\{\,[p_n(x)H_n(x)+q_n(x)F_n(x)]_{\rm I}+[p_n(x)H_n(x)]_{\rm I'}+[p_n(x)G_n(x)+q_n(x)K_n(x)]_{\rm II}+[p_n(x)G_n(x)+q_n(x)K_n(x)]_{\rm III}+[p_n(x)G_n(x)+q_n(x)K_n(x)]_{\rm IV}+[p_n(x)G_n(x)]_{\rm V}+[p_n(x)G_n(x)+q_n(x)H_n(x)]_{\rm VI}\}+\sum_n b_n(x)(\hbar\omega)^n. \tag{11}$$

Here, the x in the functions $H_n(x)$, $F_n(x)$, $G_n(x)$, and $K_n(x)$ means that every E_i and Γ_i inside these functions is a function of x. This completes the specification of our model for $Al_xGa_{1-x}As$. Equation (11) contains all of the desirable analytical features of Eq. (9) enumerated in the previous paper.[1]

III. APPLICATION TO THE OPTICAL DIELECTRIC FUNCTION OF AlAs

Before we attempt to apply Eq. (11) to the fitting of the $L(\omega_j,x_k)$ for all of the x_k, we apply Eq. (9) to $L(\omega_j,1)$ and show in detail the fitting procedure. There are several reasons for this. First, $L(\omega_j,1)$ has never

been modeled previously. The successful application of Eq. (9) to $L(\omega_j,1)$ suggests that Eq. (9), which was developed for GaAs, is applicable to the spectral data of any $Al_xGa_{1-x}As$ alloy, since AlAs is the opposite endpoint to GaAs. Second, we want to show the simple steps to follow in modeling any spectral data with Eq. (9).

The spectral data, $L(\omega_j,1)$, were taken from the results of Garriga *et al.*,[7] who measured the optical dielectric function of AlAs and reported two possible results for $L(\omega_j,1)$. The first was calculated from their data without any surface-layer correction and the second was calculated under the assumption of a 6-Å oxide layer. The first has less noise than the second, but, on the other hand, has a smaller peak value (28.2) in the E_2 complex region (around 4.5 eV) than that (30.8) of the second. Both sets of values for $L(\omega_j,1)$ were tried, but the second one was chosen for two reasons. First, a 6-Å oxide surface layer was expected to be present on physical and chemical grounds.[6] Second, a peak value of about 30 is expected[6] for AlAs using the extrapolation method from the peak values for $L(\omega_j,x_k)$ with $0\le x_k\le 0.8$.[22]

Within the Lorentzian approximation, the fitting of $L(\omega_j,1)$ is performed in three simple steps. The first step is to determine the E_i and Γ_i by minimizing the root-mean-square (rms) fractional error σ_2 defined by

$$\sigma_2^2=\tfrac{1}{4}\sum_{n=0}^{3}\sigma_{2,n}^2, \tag{12}$$

where

$$\sigma_{2,n}^2=\frac{\sum_j\{[\epsilon_2(\omega_j)]_{\rm num}^{(n)}-[L_2(\omega_j,1)]_{\rm num}^{(n)}\}^2}{\sum_j\{[L_2(\omega_j,1)]_{\rm num}^{(n)}\}^2},$$

the superscript n denotes nth-order differentiation and the subscript num indicates that the differentiation is performed numerically. The numerical differentiation is applied both to the spectral data and to the model, using the same numerical algorithm and the same energy spacing between successive points, which eliminates the errors arising from distortion by the numerical differentiation.[23] Values for the coefficients $p_{n,\nu}$ and $q_{n,\nu}$ also are determined in this step, in which a best simultaneous fit to $L_2(\omega_j,1)$ and its first three derivatives is found. In the second step the $p_{n,\nu}$ and $q_{n,\nu}$ are redetermined by minimizing $\sigma_{2,0}^2$, using the values for E_i and Γ_i determined in the first step. This is done in order to obtain a best fit of $\epsilon_2(\omega_j)$ to $L_2(\omega_j,1)$ with the E_i and Γ_i fixed at their correct values. This second step is very quick because $\epsilon(\omega)$, as in Eq. (9), is a linear function of the $p_{n,\nu}$ and $q_{n,\nu}$, so that they are determined exactly in only one iteration. The last step is to determine the b_n by minimizing

$$\sigma_{1,0}^2=\frac{\sum_j\{\epsilon_1(\omega_j)-L_1(\omega_j,1)\}^2}{\sum_j\{L_1(\omega_j,1)\}^2}, \tag{13}$$

using the values for the E_i, Γ_i, $p_{n,\nu}$, and $q_{n,\nu}$ determined in the first and second steps. Like the $p_{n,\nu}$ and $q_{n,\nu}$, the b_n are determined exactly in a single iteration.

Figure 1 shows the results of the first step in the Lorentzian fitting of $L_2(\omega_j,1)$ and its first three numerical derivatives using 29 parameters—the E_i and Γ_i at each of the seven critical points considered and a total of 15 coefficients in the polynomials $p_\nu(E)$ and $q_\nu(E)$. The rms fractional error σ_2 is 15.4%, which is large mainly due to the amplification of noise in the derivative spectra. The fit to $L_2(\omega_j,1)$ around E_0 is poor because of the contribution coming from the tail of the line shape above the E_1 critical point, which is large because of the assumption of Lorentzian line broadening. However, the value for E_0 is acceptable because the fits to the derivatives of $L_2(\omega_j,1)$ around E_0 are reasonably good.

Garriga *et al.*[7] reported values for all of the E_i from an analysis of $L(\omega_j,1)$. They fitted $[L_2(\omega_j,1)]_{\rm num}^{(2)}$ with the appropriate theoretical line shapes.[24,25] However, their method does not take account of the errors[23] due to the distortion by the numerical differentiation. Table I compares the values for E_i determined by their method to those determined by our method.[23] The values we find for the E_i are almost totally independent of whether or not a surface overlayer due to oxidization is assumed, as is shown by rows (a) and (b) of Table I. The value for E_0 in row (c) of Table I is found by Garriga *et al.*, assuming a 2D critical-point line shape; the value for $E_2(X)$ in row (c) is cited from the value of Garriga *et al.* for $E_0'+\Delta_0'$.

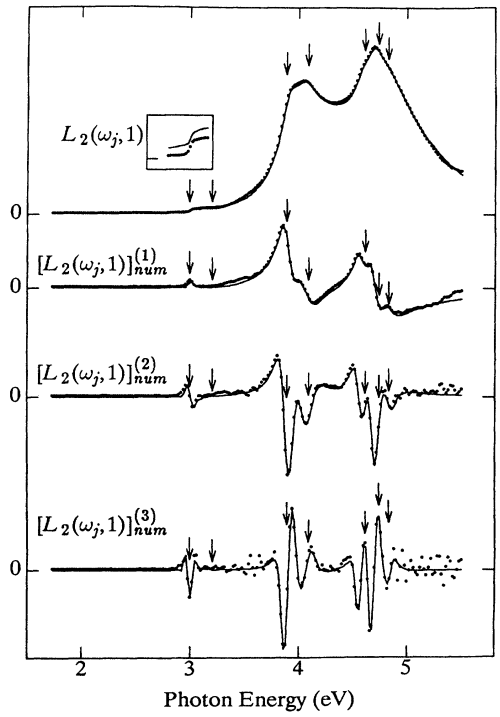

FIG. 1. Lorentzian fits to $L_2(\omega_j,1)$ and its first three numerical derivatives. The bullets show $L_2(\omega_j,1)$ and its numerical derivatives. The solid lines show the resultant fits. The inset shows the fit to $L_2(\omega_j,1)$ around E_0 with the scale expanded by a factor of 4. The arrows show the position of the seven critical points as determined by fitting.

TABLE I. Values for the critical-point energies E_i for AlAs, determined (a) from $L_2(\omega,1)$ without the surface-layer correction by our method, (b) from $L_2(\omega,1)$ with the surface-layer correction by our method, (c) by Garriga *et al.*, and (d) by Onton. The values are given in units of eV.

Class	$E_0(\Gamma)$	$E_0(\Gamma)+\Delta_0(\Gamma)$	$E_1(\Lambda)$	$E_1(\Lambda)+\Delta_1(\Lambda)$	$E_0'(\Delta)$	$E_2(X)$	$E_2(K)$
(a)	2.993	3.201	3.887	4.088	4.610	4.737	4.830
(b)	2.993	3.201	3.888	4.087	4.611	4.738	4.827
(c)	3.003		3.899	4.048	4.578	4.688	4.853
(d)	2.95		3.90	4.09	4.54	4.69	4.89

Values for the Γ_i were determined both with and without the surface-layer correction. The values for Γ_i obtained from fitting $L(\omega_j,1)$ with the surface-layer correction are slightly smaller overall than those obtained from fitting $L(\omega_j,1)$ without that correction. The value for $\Gamma(E_0)$ is much smaller than the energy spacing between data points and this could not be determined through the fit. Thus, the value for $\Gamma(E_0)$ is simply fixed at 5 meV after trying with several different values. The value for $\Gamma(E_0+\Delta_0)$ also was difficult to determine, due to the small signal-to-noise ratio in the derivative spectra, and is fixed at 40 meV. The value for $\Gamma(E_2(\Sigma))$ also was difficult to determine through the fit. The signal-to-noise ratio in $[L_2(\omega_j,1)]^{(3)}_{\rm num}$ around $E_2(\Sigma)$ is close to one. It is not clear whether the fit around the $E_2(\Sigma)$ region should follow exactly the first sharp peak or broadly cover the following several peaks. Thus, the accurate determination of $\Gamma(E_2(\Sigma))$ becomes somewhat uncertain. All of the other values for the Γ_i were obtained with confidence. The values for the Γ_i of AlAs obtained from fitting $L(\omega_j,1)$ with the surface-layer correction are given later, with those for $x_k \neq 1$.

Having found the values for the E_i and Γ_i we proceed to the second step in our fitting procedure. However, as is shown in Fig. 1, the resulting fit to $L_2(\omega_j,1)$ with purely Lorentzian broadening does not yield a good fit to $L_2(\omega_j,1)$, especially around E_0. One way to circumvent this difficulty is to perform the fit only above E_0, setting the fitting function $\epsilon_2(\omega,1)$ equal to zero below E_0, as others do.[18,19,26] Instead, we allow the line broadening to be partially Gaussian in character, introducing nonzero values for α_i in order to improve our calculation of $\epsilon_2(\omega,1)$. In principle, we should make each α_i a free parameter and determine its value by fitting $L_2(\omega_j,1)$ and its numerical derivatives simultaneously. However, we find that the values for α_i are not well determined and that any small values for the α_i above E_1 greatly improve the fit to $L_2(\omega_j,1)$, especially around E_0. In order to keep our fitting procedure simple, we use the same values for the

$$\xi_i \equiv \frac{\alpha_i}{\Gamma_i^2} \tag{14}$$

as those used to produce the best fit for GaAs in the previous paper.[1] Those values are listed in Table II. The reason for making ξ_i the same, rather than the α_i, is explained in Sec. V.

Having chosen values for the ξ_i, we repeated steps one and two to find a new best fit to $L_2(\omega_j,1)$. This fit was clearly better than the best Lorentzian fit shown in Fig. 1. In finding this fit, we found that many of the coefficients $p_{n,\nu}$ and $q_{n,\nu}$ were so small that the corresponding contributions to $\epsilon_2(\omega,1)$ were unimportant. Upon allowing only 16 of the $p_{n,\nu}$ and $q_{n,\nu}$ to be nonzero, for a total of 29 free parameters, we found the fit to $L_2(\omega_j,1)$ shown in Fig. 2(a). The corresponding best-fit values of the $p_{n,\nu}$ and $q_{n,\nu}$ are given in Table III. The resultant rms fractional deviation in the fit to $L_2(\omega_j,1)$ is $\sigma_{2,0}=0.95\%$. An increase in the number of free coefficients $p_{n,\nu}$ and $q_{n,\nu}$ results in only a small decrease in $\sigma_{2,0}$. We believe that this remaining small deviation results in part from inexactness in our treatment of broadening and in part from the neglect of several critical points in the high-energy end of our fitting range and from the neglect of critical points above that range. However, this deviation is substantially smaller than the rms deviations found in fits made using other models.

The last step is to calculate $\epsilon_1(\omega,1)$. The stars in Fig. 2(b) show the zero-parameter calculation of $\epsilon_1(\omega,1)$ with $\sigma_{1,0}=20.3\%$, with all of the parameters fixed at the values obtained above from fitting $L_2(\omega_j,1)$. Notice that the difference between $L_1(\omega_j,1)$ and this calculated $\epsilon_1(\omega,1)$ does not contain any sharp structure and gradually increases as the photon energy increases. The substantial difference between them arises from the contributions of critical points above 6 eV. Those critical points were neglected in the calculation of $\epsilon_2(\omega,1)$. We approximate the contribution of those critical points to $\epsilon_1(\omega,1)$ by the power series $\sum b_n(\hbar\omega)^n$. The fit to $L_1(\omega_j,1)$ is greatly improved by making the b_n free parameters, even for $n\leq 2$. We limit the maximum value for n to 2, because the unbiased estimator is minimized for that choice. The values $b_0=4.29$, $b_1=-2.63$, and $b_2=0.534$ lead to the small rms fractional error $\sigma_{1,0}=1.61\%$. With $\epsilon(\omega,1)$ known, all other optical constants such as $R(\omega,1)$,

TABLE II. Values for the ξ_i taken from Ref. 1 and assumed to be independent of x.

Critical point	$E_0(\Gamma)$	$E_0(\Gamma)+\Delta_0(\Gamma)$	$E_1(\Lambda)$	$E_1(\Lambda)+\Delta_1(\Lambda)$	$E_0'(\Delta)$	$E_2(X)$	$E_2(\Sigma)$
ξ_i	7200	2000	3	1	0	0	0

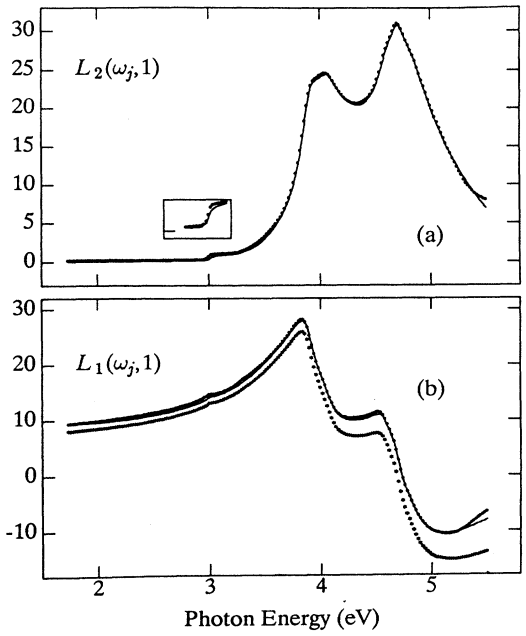

FIG. 2. Mixed Gaussian and Lorentzian fits to (a) $L_2(\omega_j,1)$ and (b) $L_1(\omega_j,1)$. The bullets and the solid lines show $L(\omega_j,1)$ and the resultant fits, respectively. The inset in (a) shows the fit to $L_2(\omega_j,1)$ around E_0 with the scale expanded by a factor of 4. The stars in (b) show the zero-parameter calculation with the parameters used to fit $L_2(\omega_j,1)$.

$N(\omega,1)$, and $\alpha(\omega,1)$ are easily calculated by the use of the appropriate optical formulas.

IV. DETERMINATION OF $E_i(x)$ AND $\Gamma_i(x)$

The calculation of $\epsilon(\omega,x)$ with Eq. (11) requires a knowledge of the critical-point energies $E_i(x)$ and linewidths $\Gamma_i(x)$ as a function of x. It is possible to obtain such knowledge from the literature, but it is not sufficient, nor accurate, as is discussed below. On the other hand, our model is capable of determining the values of the E_i and Γ_i directly and accurately from $L(\omega_j,x_k)$.[27] Following the first step in the previous section, we first determine the values of the $E_i(x_k)$ and $\Gamma_i(x_k)$ by fitting $L(\omega_j,x_k)$ and its numerical derivatives at each x_k at which $L(\omega_j)$ is known. Then, we fit these values to low-order polynomials to obtain $E_i(x)$ and $\Gamma_i(x)$.

Berolo and Woolley[28] reported $E_i(x)$ for $Al_xGa_{1-x}As$ from the analysis of electroreflectance (ER) data. They determined the E_i values from the photon energy at the peak of each critical-point structure. Thus, their E_i values contain uncertainties approximately of the order of the linewidth at each critical point. Also, they reported two possible critical-point energies for $E_1(\Lambda)$ and $E_1(\Lambda)+\Delta_1(\Lambda)$. Aspnes *et al.*[6] applied their new method[29] to $L(\omega_j,x_k)$ data and reported values for E_0 and $E_1(\Lambda)$, but did not report the values of the rest of the critical-point energies. Recently, Logothetidis *et al.*[30] reported values for the $E_i(x)$ between 4.0 and 5.5 eV, but only at low temperature. None of them reported values for the $\Gamma_i(x)$, which are not available in the literature.

Table IV shows the values for the E_i obtained from following the first step in Sec. III assuming Lorentzian broadening. The values found for the E_i are very nearly independent of the assumed nature of the broadening. All the critical point energies below the E_2 complex region are determined with confidence except those of $E_0(\Gamma)+\Delta_0(\Gamma)$. Those are not well known because the signal-to-noise ratio in the derivative spectra around the $E_0+\Delta_0$ region decreases as n increases and becomes less than one for $n=3$. The values for the E_i in the E_2 complex region are hard to determine accurately because of the closely packed critical-point structure in that region. Of the three critical-point energies in this region, those for $E_2(X)$ are most uncertain for two reasons. First, the

TABLE III. Values for $p_{n,\nu}$ and $q_{n,\nu}$ obtained by minimizing Eq. (13). The values are multiplied by $8\pi\hbar^2e^2/m^2$.

Region	p_0	p_1	p_2	q_0	q_1	q_2
I	-396.0	116.2	0.0	451.0	-130.7	0.0
I′	2.9	0.0	0.0	0.0	0.0	0.0
II	48858.0	-11641.7	0.0	-7462.4	0.0	0.0
III	1736.8	-336.3	0.0	-328.0	0.0	0.0
IV	-429.3	135.9	0.0	0.0	0.0	0.0
V	234.6	0.0	0.0	0.0	0.0	0.0
VI	289.0	0.0	0.0	-265.7	0.0	0.0

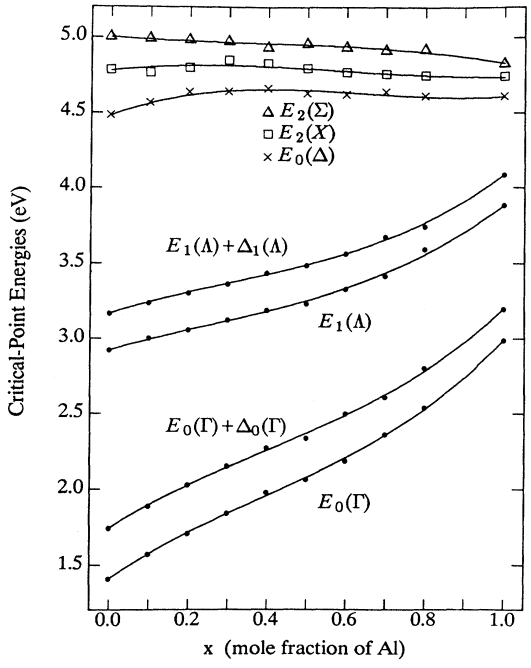

FIG. 3. The seven critical-point energies of $Al_xGa_{1-x}As$. The discrete symbols show the values found by fitting the $L(\omega_j,x_k)$. The solid lines show the least-square cubic-polynomial fits to those values.

TABLE IV. Values of the critical-point energies E_i determined by minimizing Eq. (12) using the first step described in Sec. III. The values are given in units of eV.

x	$E_0(\Gamma)$	$E_0(\Gamma)+\Delta_0(\Gamma)$	$E_1(\Lambda)$	$E_1(\Lambda)+\Delta_1(\Lambda)$	$E_0'(\Delta)$	$E_2(X)$	$E_2(\Sigma)$
0.0	1.410	1.746	2.926	3.170	4.483	4.781	5.002
0.1	1.574	1.889	3.005	3.241	4.566	4.761	4.989
0.2	1.711	2.030	3.059	3.306	4.635	4.793	4.982
0.3	1.844	2.154	3.125	3.366	4.639	4.844	4.973
0.4	1.981	2.275	3.193	3.440	4.658	4.823	4.931
0.5	2.068	2.338	3.237	3.490	4.628	4.790	4.957
0.6	2.191	2.501	3.334	3.566	4.620	4.763	4.933
0.7	2.360	2.610	3.419	3.677	4.636	4.752	4.913
0.8	2.541	2.805	3.596	3.747	4.610	4.743	4.918
1.0	2.993	3.201	3.888	4.087	4.611	4.739	4.827

strength of $E_2(X)$ in the derivative spectra below $x = 0.3$ is very weak compared to that of the other critical points nearby. Second, the strength of $E_2(X)$ in the derivative spectra increases above $x = 0.3$, but there appear to be two dominant critical-point structures around $E_2(X)$, not one. This is because the magnitude of the structure at $E_2(X)+\Delta_2(X)$, which was set to zero in our model based on the band structure[20] of GaAs, is not negligible for AlAs.[30] This implies an uncertainty in our value for $E_2(X)$ about half the magnitude of $\Delta_2(X)$.

The discrete points in Fig. 3 show the values for the E_i listed in Table IV. Interestingly, the variation of $E_0'(\Delta)$ below $x = 0.3$ is very different from that above $x = 0.3$, which is coincident with the change from a direct band gap to an indirect band gap. Also, the value for $E_2(\Sigma)$ at $x = 1$ is a little lower than the value which can be extrapolated from the values below $x = 0.8$. The value given for $E_2(\Sigma)$ for AlAs by Onton[31] (refer to Table I) does agree with the extrapolated value. We can use his value, but for consistency we did not use his value for $E_2(\Sigma)$ at $x = 1$; instead, we used our value, which is accurately determined from fitting $L(\omega_j, 1)$.

There are several possible ways to obtain the E_i as a function of x from our values for the $E_i(x_k)$. Conventionally, the values $E_i(x_k)$ are fitted as a quadratic function of x to obtain the bowing parameter. However, it has been pointed out[6] that $E_0(x)$ cannot be described over the entire range of x by a simple quadratic equation. The critical-point energies in the E_2 complex region often are fitted by a linear function.[30] Since our main purpose in fitting $E_i(x_k)$ is to calculate the $E_i(x)$ as accurately as possible, we use the cubic equation,

$$E_i(x) = E_i(0) + [E_i(1) - E_i(0)]x + (c_0 + c_1 x)x(1-x) \tag{15}$$

to fit the $E_i(x_k)$ for all critical points. Because the values of the E_i are determined most accurately for $x = 0$ and $x = 1$ and because no errors in x occur at those points, the values of the $E_i(x)$ are fixed at those points. This leaves only two fitting parameters, c_0 and c_1, which are determined by fitting the values of $E_i(x_k)$ at the eight x_k points not equal to zero or one. The values for c_0 and c_1 determined from this fit are listed in Table V. The solid lines in Fig. 3 show the resultant fits.

Table VI gives the values for all of the Γ_i except $\Gamma(E_0+\Delta_0)$. The accurate determination of the Γ_i is generally more difficult than that of the E_i. The values for $\Gamma(E_0)$ below $x = 0.4$ are much smaller than the energy spacing between data points and are arbitrarily fixed at 5 meV. The values for $\Gamma(E_0+\Delta_0)$ are very hard to determine because of the small signal-to-noise ratio in the derivative spectra, and are fixed at 40 meV for all x. The values for all the other linewidths are obtained with confidence.

The discrete points in Fig. 4 show the values for $\Gamma_i(x_k)$ listed in Table VI. One sees that the values for $\Gamma(E_0)$, $\Gamma(E_1)$, and $\Gamma(E_1+\Delta_1)$ at $x = 0.8$ are much higher than the expected values. This clearly indicates that the quality of the samples for $x = 0.8$ is very poor, so that $L(\omega_j, 0.8)$ is not as reliable as $L(\omega_j, x_k)$ for the other values of x_k.

We use the equation

$$\Gamma_i(x) = \Gamma_i(0) + [\Gamma_i(1) - \Gamma_i(0)]x + (c_0 + c_1 x)x(1-x) \tag{16}$$

to fit the values for the $\Gamma_i(x_k)$. This equation is exactly analogous to Eq. (15), which we use to fit the $E_i(x_k)$. Table VII gives the values for c_0 and c_1 obtained from this fit. In fitting the values for $\Gamma(E_0)$, $\Gamma(E_1)$, and $\Gamma(E_1+\Delta_1)$, the values at $x = 0.8$ are not included, since they are highly unreliable. The solid lines in Fig. 4 show the resultant fits.

TABLE V. Values of c_0 and c_1 used to obtain the $E_i(x)$ in Eq. (15).

Class	$E_0(\Gamma)$	$E_0(\Gamma)+\Delta_0(\Gamma)$	$E_1(\Lambda)$	$E_1(\Lambda)+\Delta_1(\Lambda)$	$E_0'(\Delta)$	$E_2(X)$	$E_2(\Sigma)$
c_0	0.2242	0.1931	-0.2124	-0.0734	0.8574	0.3260	-0.0336
c_1	-1.4235	-1.2160	-0.7850	-0.9393	-0.7413	-0.1993	0.3606

TABLE VI. Values of the critical-point linewidths, Γ_i, determined by minimizing Eq. (12) using the first step described in Sec. III. The values are given in units of meV.

x	$\Gamma(E_0)$	$\Gamma(E_1)$	$\Gamma(E_1+\Delta_1)$	$\Gamma(E_0')$	$\Gamma(E_2(X))$	$\Gamma(E_2(\Sigma))$
0.0	5.0	34.6	78.9	82.7	111.9	125.6
0.1	5.0	40.1	77.9	95.7	109.4	133.2
0.2	5.0	44.5	91.7	113.4	120.8	135.5
0.3	5.0	60.3	109.2	114.8	84.4	89.2
0.4	5.0	63.8	113.2	102.4	65.7	63.8
0.5	9.5	79.6	123.8	102.5	73.7	82.7
0.6	17.5	81.2	163.0	84.7	56.4	69.1
0.7	15.2	104.0	166.7	62.3	46.0	57.9
0.8	35.7	175.9	248.3	53.4	52.6	65.4
1.0	5.0	75.7	149.3	48.2	43.3	64.1

V. OPTICAL PROPERTIES AS A FUNCTION OF ω AND x

Having found the $E_i(x)$ and $\Gamma_i(x)$ for all critical points as a function of x, we proceed to the second step in our fitting procedure. Because we know that the Lorentzian approximation does not yield an accurate representation for $\epsilon_2(\omega, x)$, we immediately introduce nonzero values for the parameters α_i, so as to obtain a Gaussian component to the broadening. For simplicity, and in order not to introduce more variable parameters, we fix the values of the α_i's using the values found for GaAs in our earlier paper.[1] As in finding $\epsilon(\omega, 1)$, for all x we set $\xi_i \equiv \alpha_i/\Gamma_i^2$ equal to its value for $\epsilon(\omega, 0)$. We choose ξ_i constant rather than α_i because of the form of D_i in Eq. (10); the exponent in that expression for D_i is proportional to ξ_i, not α_i, for fixed $E_i - \hbar\omega$. This choice was found to yield good fits to the measured $L(\omega_j, x_k)$. Table II shows the values for the ξ_i, which were obtained by fitting the spectral data of GaAs.

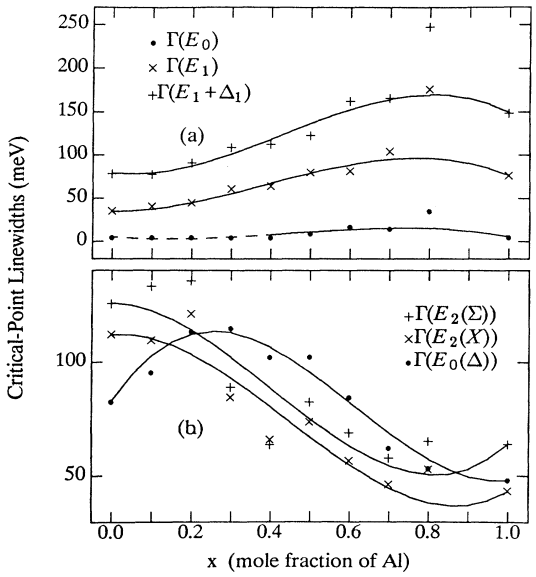

FIG. 4. The critical-point linewidths of $Al_xGa_{1-x}As$. The discrete symbols show the values for Γ_i found by fitting the $L(\omega_j, x_k)$ except those under the dashed line (a) below the E_2 complex region and (b) in the E_2 complex region. The solid lines show the least-square cubic-polynomial fits to those values.

Now we are ready to complete the calculation of $\epsilon(\omega, x)$ by obtaining the $p_n(x)$, $q_n(x)$, and $b_n(x)$ in Eq. (11). The $p_n(x)$ and $q_n(x)$ can be obtained by minimizing the rms fractional error Σ_2, defined by

$$\Sigma_2^2 = \sum_k \left[\frac{\sum_j \{\epsilon_2(\omega_j, x_k) - L_2(\omega_j, x_k)\}^2}{\sum_j \{L_2(\omega_j, x_k)\}^2} \right]. \quad (17)$$

One can leave as many of the $p_{n\nu}(x_k)$ and $q_{n\nu}(x_k)$ free at any given composition x_k as one desires, with the remainder of the $p_{n\nu}(x_k)$ and $q_{n\nu}(x_k)$ set to zero. Allowing too many free parameters yields values which are not meaningful and are not smoothly varying functions of x. On the other hand, allowing too few free parameters seriously worsens the fit to $L(\omega_j, x_k)$. We have chosen 21 of the $p_{n\nu}$ and $q_{n\nu}$ *in toto* to be free for each x_k, as is shown in Table VIII, with these parameters relabeled as c_k, $k = 1, \ldots, 21$. None of the $p_\nu(E)$ were allowed to be higher than quadratic order, and none of the $q_\nu(E)$ were allowed to be nonlinear. We now expressed each c_k (each $p_{n\nu}$ and $q_{n\nu}$) as a polynomial in x according to the equation

$$c_k(x) = \sum_{m=0}^{m=N_k} c_{km}(x - 0.5)^m, \quad (18)$$

where the c_{km} are composition-independent parameters. N_k gives the maximum order of the polynomial for each $c_k(x)$. Notice that $\epsilon(\omega, x)$ is linear in the c_{km}. Thus, all of the c_{km} are determined by minimizing Eq. (17) in a single iteration. We find that the maximum number 3 for N_k is sufficient to produce a reasonable fit to the entire $L_2(\omega_j, x_k)$. If all of the N_k are set equal to 3, the total number of free parameters c_{km} is $84 = 4 \times 21$. The rms fractional error Σ_2 always decreases as the total number of parameters increases. We try to obtain the minimum value for Σ_2 with the least number of parameters. If there is not much improvement in Σ_2 after adding more parameters, those parameters are discarded. Table IX shows the values for c_{km} with a total of 75 free parameters, which results in $\Sigma_2 = 1.2\%$.

TABLE VII. Values of c_0 and c_1 used to obtain the $\Gamma_i(x)$ in Eq. (16).

Class	$\Gamma(E_0)$	$\Gamma(E_1)$	$\Gamma(E_1+\Delta_1)$	$\Gamma(E_0')$	$\Gamma(E_2(X))$	$\Gamma(E_2(K))$
c_0	0.0380	-0.0414	-0.1164	0.3000	0.0818	0.0588
c_1	0.0000	0.2776	0.4169	-0.3592	-0.2493	-0.2766

Figure 5(a) compares our fitted model for $\epsilon_2(\omega,x)$, shown by the solid curves, with $L_2(\omega_j,x_k)$, shown by discrete symbols, for x_k = 0.0, 0.3, 0.7, and 1.0. As is shown by the figure, the agreement between $L_2(\omega_j,x_k)$ and $\epsilon_2(\omega,x)$ is excellent for these compositions. For $x_k = 0.8$, which is not shown in the figure, the agreement is not as good; in particular, $\epsilon_2(\omega,0.8)$ attains a maximum value of 27.3 in the E_2 region, whereas $L_2(\omega_j,0.8)$ only reaches a maximum of 26.87. However, as has been discussed by Aspnes *et al.*,[6] surface oxidation probably substantially reduces the maximum of $L_2(\omega_j,0.8)$. Thus, we believe that $\epsilon_2(\omega,0.8)$ probably is more accurate than $L_2(\omega_j,0.8)$.

The final step in the determination of $\epsilon(\omega,x)$ is the calculation of $\epsilon_1(\omega,x)$, which is done by finding the $b_n(x)$ in Eq. (11). The $b_n(x)$ are obtained by minimizing the rms fractional error Σ_1, defined by

$$\Sigma_1^2 = \sum_k \left[\frac{\sum_j \{\epsilon_1(\omega_j,x_k) - L_1(\omega_j,x_k)\}^2}{\sum_j \{L_1(\omega_j,x_k)\}^2} \right]. \quad (19)$$

We approximate the $b_n(x)$ as cubic functions of x,

$$b_n(x) = \sum_{m=0}^{m=N_n} b_{nm}(x-0.5)^m, \quad (20)$$

and determine the values of the b_{nm} by minimizing Eq. (19). Table X shows the resultant values for the b_{nm}, which yield Σ_1 = 2.37%. Figure 5(b) compares the resultant $\epsilon(\omega,x_k)$ with $L_1(\omega_j,x_k)$ for x_k=0.0, 0.3, 0.7, and 1.0.

Although Aspnes *et al.*[6] reported values for $L(\omega_j,0.9)$, those values were not considered to be as accurate as $L(\omega_j,x_k)$ for $0.0 \le x_k \le 0.8$. Because the sample surface with this high aluminum composition was very reactive with the atmosphere, an ideal surface could not be obtained by chemical treatment. His values for $L_2(\omega_j,0.9)$ were distorted by a surface film, as is evidenced by the nonzero values of $L_2(\omega_j,0.9)$ at low energies and the relatively low value of its maximum in the E_2 region. On the other hand, our model yields reliable values for $\epsilon(\omega,x)$ for all x and thus can be used to calculate $L(\omega,x)$ for any x. On Fig. 6 the dots, times signs, and solid curve show $L(\omega_j,0.8)$, $L(\omega_j,1.0)$, and $\epsilon_2(\omega,0.9)$, respectively. In contrast to the experimental $L_2(\omega_j,0.9)$, $\epsilon_2(\omega,0.9)$ shows reliable behavior at all ω.

The other optical properties of $Al_xGa_{1-x}As$ are easily calculated from $\epsilon(\omega,x)$. We find $N(\omega,x)$ and $\alpha(\omega,x)$ from

$$N(\omega,x) = \sqrt{\epsilon(\omega,x)} \quad (21)$$

and

$$\alpha(\omega,x) = \frac{4\pi}{\lambda}k(\omega,x) = \frac{2\omega}{c}k(\omega,x), \quad (22)$$

where λ is the wavelength in vacuum. Figure 7 compares $N(\omega,x_k)$ to $\sqrt{L(\omega_j,x_k)}$, with x_k=0.0, 0.3, 0.7, and 1.0. The rms fractional difference between $N(\omega,x)$ and $\sqrt{L(\omega_j,x_k)}$ is only 1%.

Let us compare our results with others in the literature. Recently, Adachi[18,32] calculated the optical properties of $Al_xGa_{1-x}As$ with his model. Our model produces much better results than his. In particular, our calculation of $\epsilon_1(\omega,x)$ is much better than his, which leads our $n(\omega,x)$ to be much better. More recently, Jenkins[19] improved the

TABLE VIII. Selected parameters c_k among the $p_{n,\nu}$ and $q_{n,\nu}$; the zero values indicate parameters not allowed to be free, but fixed at zero.

Region	p_0	p_1	p_2	q_0	q_1	q_2
I	c_1	c_2	c_3	c_4	c_5	0
I′	c_6	0	0	0	0	0
II	c_7	c_8	0	c_9	0	0
III	c_{10}	c_{11}	c_{12}	c_{13}	c_{14}	0
IV	c_{15}	c_{16}	c_{17}	0	0	0
V	c_{18}	0	0	0	0	0
VI	c_{19}	0	0	c_{20}	c_{21}	0

TABLE IX. Values for the c_{km}. The values are multiplied by $8\pi\hbar^2e^2/m^2$. The zero values indicate parameters not allowed to be free, but fixed at zero.

c_k	c_{k0}	c_{k1}	c_{k2}	c_{k3}
c_1	2094.3	-16.9	-3006.9	0.0
c_2	-883.1	193.3	1585.9	0.0
c_3	80.3	-30.9	-186.9	0.0
c_4	-1118.7	168.4	1688.4	0.0
c_5	270.9	-103.5	-515.7	0.0
c_6	0.9	0.0	0.0	0.0
c_7	8367.0	17902.0	2672.8	-14769.0
c_8	-2296.2	-4516.4	491.2	5166.6
c_9	-1651.6	-3138.0	36.4	3241.6
c_{10}	5181.7	-7300.5	23539.0	11526.0
c_{11}	-1159.6	2655.4	-8900.2	-1299.1
c_{12}	27.5	-245.6	784.3	-170.8
c_{13}	-2480.5	2394.5	-9842.4	-4818.0
c_{14}	337.3	-423.5	2254.0	394.1
c_{15}	-195490.0	214390.0	-594970.0	-3529900.0
c_{16}	83395.0	-90786.0	254430.0	1505400.0
c_{17}	-8882.6	9604.3	-27205.0	-160480.0
c_{18}	168.0	-60.8	257.0	0.0
c_{19}	164.2	97.4	172.1	575.9
c_{20}	-465.9	-209.7	-354.1	-2924.5
c_{21}	64.3	20.9	28.1	386.2

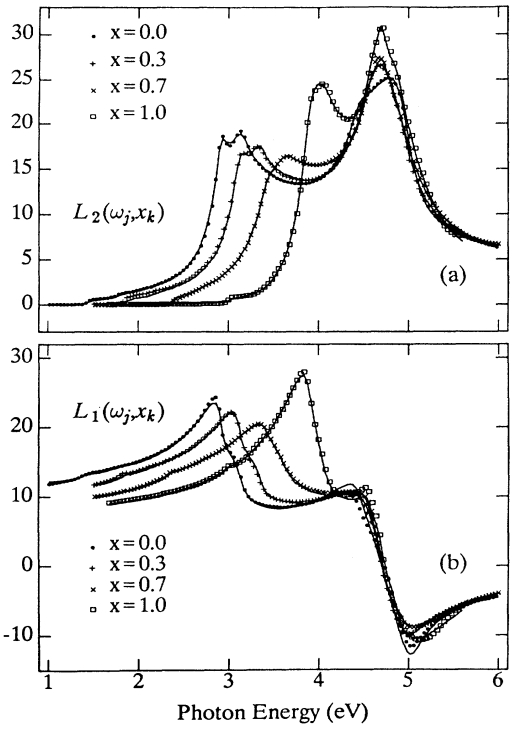

FIG. 5. Comparison of $L(\omega_j, x_k)$ to $\epsilon(\omega, x)$, but only with $x = 0.0, 0.3, 0.7$, and 1.0 for the sake of clarity. The discrete symbols show $L_2(\omega_j, x_k)$ in steps of 40 meV, and the solid lines show the resultant fits.

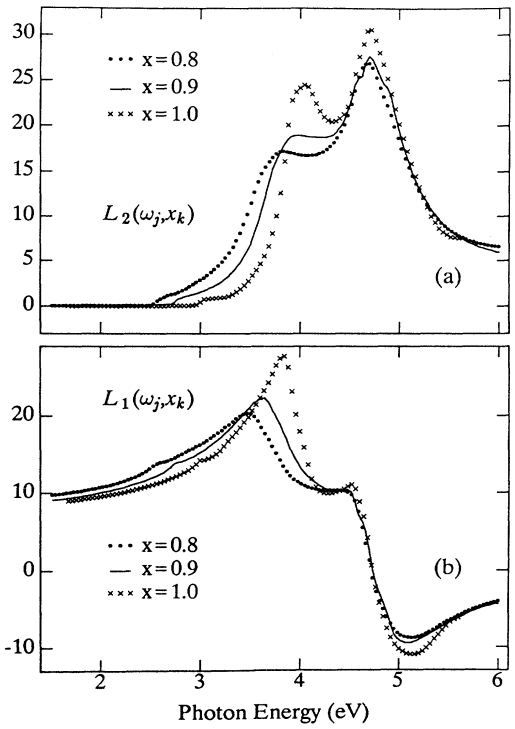

FIG. 6. Calculation of $\epsilon(\omega, 0.9)$. The solid lines show the calculated values for (a) $\epsilon_2(\omega, 0.9)$ and (b) $\epsilon_1(\omega, 0.9)$. The bullet and times signs show $L(\omega_j, 0.8)$ and $L(\omega_j, 1.0)$ in steps of 40 meV, respectively.

TABLE X. Values for the b_{nm}.

b_n	b_{n0}	b_{n1}	b_{n2}	b_{n3}
b_0	0.74225	-1.28150	2.49650	-0.28206
b_1	-0.11830	0.25810	-2.35070	3.01670
b_2	0.07550	0.01391	0.39486	-0.60463

model by Adachi[26] and calculated the optical properties of $Al_xGa_{1-x}As$, focusing on $n(\omega, x)$ in the photon range between 1.0 and 3.0 eV. Over this small energy range, his values for $n(\omega, x)$ with $x \leq 0.8$ have a rms fractional error of only 1%, which is much better than the 9.6% rms fractional error in the values of Adachi. However, his values for $n(\omega, 1)$ from 1.0 to 3.0 eV have a 6% rms fractional error.

The best previous results were obtained by Terry.[13] He improved the harmonic oscillator (HO) model and fitted $L(\omega_j, x_k)$ with his improved model. He used nine harmonic oscillators, with a total of 36 parameters to fit $L(\omega_j, x_k)$ for each x_k. Thus, he used a total of 144 parameters (36×4) to fit $L(\omega_j, x_k)$ over the range $1.5 \leq \hbar\omega \leq 5.0$ eV and $0 \leq x_k \leq 0.8$. The rms fractional difference between his $\epsilon(\omega, x)$ and $L(\omega_j, x_k)$ is less than 3% for each x_k. We use seven critical points with a total of 37 parameters to fit $L(\omega_j, x_k)$ for each x_k. We use a total of 119 parameters (see Tables V, VII, II, IX, and X) to

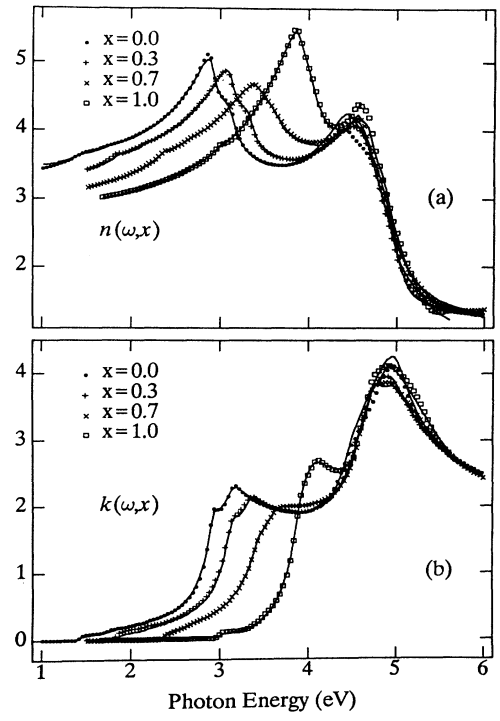

FIG. 7. Comparison of $\sqrt{L(\omega_j, x_k)}$ to $N(\omega, x)$, but only with $x = 0$, 0.3, 0.7, and 1.0 and for the sake of clarity. The discrete symbols show the real and imaginary parts of $\sqrt{L(\omega_j, x_k)}$ in steps of 40 meV, and the solid lines show the calculated values for (a) $n(\omega, x)$ and (b) $k(\omega, x)$.

fit $L(\omega_j, x_k)$ over the full range of photon energies from 1.5 to 6.0 eV and for all x from zero to one.[27] The rms fractional difference between our $\epsilon(\omega, x)$ and $L(\omega_j, x_k)$ is less than 2.5% for each x_k. Thus, our results are only slightly better than his, if one's major concern is to model $L(\omega_j, x_k)$ as closely as possible with $\epsilon(\omega, x)$. Also, the analytic form of his model is much simpler than that of ours. On the other hand, our model for $\epsilon(\omega, x)$ satisfies all of the required analytic properties for the optical dielectric function, whereas his model does not. Thus, our model is capable of predicting $\epsilon(\omega, x)$ outside the range of available spectral data with much greater accuracy than his. In particular, our model allows the accurate calculation of $\epsilon(\omega, x)$ and $n(\omega, x)$ in the range below 1.5 eV and well above the highest phonon frequencies, whereas the model of Terry does not.

The ability of our model to allow accurate calculations of $\epsilon(\omega, x)$ and $n(\omega, x)$ below the range of available spectral data is a great advantage. One of the most important factors in heterostructure lasers and optoelectronic devices is the refractive index. Most active regions of optical devices based on GaAs/$Al_xGa_{1-x}As$ are around 0.9 μm (1.4 eV) in wavelength. Because optical data giving $L(\omega_j, x_k)$ or $n(\omega_j, x_k)$ is not available below 1.2 eV for x_k different from zero or one and is not available below 1.5 eV for $0.38 < x < 1$, values for $n(\omega, x)$ in this region must be obtained by extrapolation from higher energies. Such extrapolation requires a model for $\epsilon(\omega, x)$ or $n(\omega, x)$. Because our model satisfies all of the required analytic properties of $J(\omega, x)$ and of $\epsilon(\omega, x)$, it yields much better extrapolations to lower energies than do any of the other existing models.

However, there are two problems in the use of even our model to find $n(\omega, x)$ for $\hbar\omega < 1.5$ eV from values of $L(\omega_j, x_k)$ for $\hbar\omega_j \geq 1.5$ eV. The first is simple and could be readily overcome. It is that the term

$$b_0(x) + b_1(x)\hbar\omega + b_2(x)(\hbar\omega)^2 \tag{23}$$

which we use to represent the effect of critical points above 6 eV on $\epsilon_1(\omega, x)$ is not sufficiently accurate and does not give a good extrapolation of that effect to lower energies. A term of the form

$$\sum_i \frac{c_i(x)}{E_i(x)^2 - (\hbar\omega)^2}, \tag{24}$$

where each $E_i > 6$ eV would be more physical and would give better results, although it would be somewhat more difficult to find the best values of the c_i's and E_i's, even if one considered only one energy E_i, than it is to find b_0, b_1, and b_2. The second difficulty is more fundamental and has nothing to do with our model. It is that the $L(\omega_j)$ obtained from spectroscopic ellipsometry data is not a perfect representation of the optical dielectric function $\epsilon(\omega)$ for a bulk material. For GaAs and AlAs the values of $L(\omega_j)$ are inconsistent with measured values of $n(\omega_j)$ over the energy ranges for which both sets of values are available. As has been discussed by the authors in a previous paper,[1] that difficulty arises at least in part from the fact that SE is very surface sensitive and that the electron wave functions must vanish at a semiconductor surface, so that the near-surface region is optically different from the bulk. It also can arise at least in part from imperfect sample surfaces.

Both of these problems can be mostly overcome by the simple expedient of replacing the term

$$\delta\epsilon_1 \equiv b_0(x) + b_1(x)\hbar\omega + b_2(x)(\hbar\omega)^2 \tag{25}$$

by the constant 0.8 for all values of x. The result of this simple substitution is shown in Fig. 8. It is clear that one could obtain an almost perfect fit by replacing $\delta\epsilon_1$ by the term

$$(d_{00} + d_{01}x) + (d_{10} + d_{11}x)\hbar\omega, \tag{26}$$

with the values of the d_{mn}'s determined by fitting $n(\omega_j, 0)$ and $n(\omega_j, 1)$. Of course, our model is valid only for $\hbar\omega$ substantially greater than the highest phonon energies for any given material, because lattice vibrations are not included in our model. However, Fig. 8 clearly shows that our model gives good agreement with the available experimental data over that range of energies. This is possible because our model incorporates the proper analytical properties of $\epsilon(\omega, x)$ below and above the band gap. The solid lines in Fig. 8 were obtained only from the fitting of $L(\omega_j, x_k)$ for $\hbar\omega_j > 1.5$ eV and were not obtained from fittings over the energy range shown in Fig. 8.

Of course, it is always possible to fit the spectral data below 1.5 eV if the data are available. Casey, Sell, and Panish[33] have measured the refractive indices of $Al_xGa_{1-x}As$ with $0 \leq x \leq 0.38$ from 1.2 and 1.8 eV. Fern and Onton[34] measured the refractive indices of AlAs from 0.5 to 2.2 eV. Afromowitz[35] calculated $n(\omega, x)$ be-

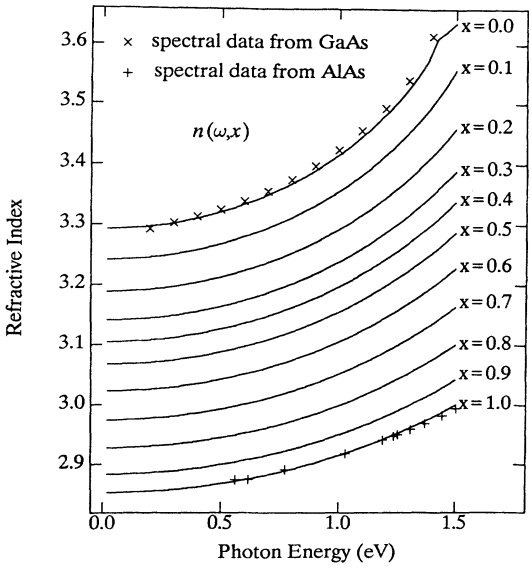

FIG. 8. Calculated values for $n(\omega, x)$ below 1.5 eV. The solid lines show the values calculated as described in the text. The times and plus signs are the measured values of the refractive indices for GaAs and AlAs, respectively.

low the band edge with a parametrized model, but had to use the composition as a fitting parameter, in order to obtain good agreement with the spectral data. Recently, Adachi[17] used his model to fit these spectral data and was able to obtain good agreement with $n(\omega_j, x_k)$ data. However, our model is the first which has been shown to predict $n(\omega, x)$ below the band gap from the spectroscopic data at higher photon energies, rather than just to be able to fit $n(\omega_j, x_k)$ data.

VI. DISCUSSION AND CONCLUSIONS

We have shown that our model produces a fit to $L(\omega_j, x_k)$ better than does any previous model. Consequently, it yields better results for $\epsilon(\omega, x)$ than does any previous model. Our model is unique in that it both determines the values for E_i and Γ_i accurately and provides an accurate fit to $L(\omega_j, x_k)$. No previous model performs both of those functions. In addition, our model contains all the correct analytical properties of $\epsilon(\omega, x)$ as was fully discussed in Ref. 1.

However, despite the great successes of the model presented here, it is necessary to issue a caveat with respect to the use of SE data to find $\epsilon(\omega)$ for any semiconductor, using any model. As was pointed out in Sec. V and was discussed in Ref. 1, the experimental $L(\omega_j)$ determined from SE data does not correspond well to the true bulk dielectric function. This is because the vanishing of the electronic wave functions at the surface of a semiconductor modifies the local dielectric function near the surface. This effect causes a rotation in phase of the measured $L(\omega_j)$. This effect must be taken into account if one is to obtain a highly accurate $\epsilon(\omega)$ for the bulk. The correction of this effect will be the subject of another paper.

One obvious application of the model used here would be to calculate $\epsilon(\omega, x)$ for other alloy systems, such as HgCdTe,[36,37] GaInAsP,[38] CdHgSe,[39] InGaAs,[40,41] ZnSSe, and so on by fitting $L(\omega_j, x_k)$ for those systems. We plan to do so in the future. Another important application would be to express the dielectric function of any semiconductor as a function of temperature. The dielectric function of GaAs as a function of temperature between 20 and 750 K has been measured by Lautenshlager *et al.*[21] Adachi[42] has obtained an analytical fit to that data, using his most recent model. Recently, Yao, Snyder, and Woollam[43] measured the dielectric function of GaAs as a function of temperature between room temperature and 900 K and used a HO model in order to express their spectral data as an analytic function of ω and T. Our model should be able to accurately model the spectral data obtained with the variation of temperature, preserving all of the advantages we found it to possess in Ref. 1 and in this paper.

ACKNOWLEDGMENTS

The authors are grateful to Dr. Aspnes and Dr. Garriga, who generously provided us with the digitized data, and acknowledge the Defense Advanced Research Projects Agency for its support under ONR Contract No. N00014-89-J-3165.

*Present address: Naval Research Laboratory, Code 6680, Washington, D.C. 20375-5345.

[1] C. C. Kim, J. W. Garland, H. Abad, and P. M. Raccah, Phys. Rev. B **45**, 11 749 (1992).
[2] D. E. Aspnes and A. A. Studna, Phys. Rev. B **27**, 985 (1983).
[3] H. R. Philipp and H. Ehrenreich, Phys. Rev. **129**, 1550 (1963).
[4] M. Erman, J. B. Theeten, N. Vodjdani, and Y. Demay, J. Vac. Sci. Technol. B **1**, 328 (1983).
[5] F. Wooten, *Optical Properties of Solids* (Academic, New York, 1972).
[6] D. E. Aspnes, S. M. Kelso, R. A. Logan, and R. Bhat, J. Appl. Phys. **60**, 754 (1986).
[7] M. Garriga, P. Lautenschlager, M. Cardona, and K. Ploog, Solid State Commun. **61**, 157 (1987).
[8] D. E. Aspnes, W. E. Quinn, and S. Gregory, Appl. Phys. Lett. **57**, 2707 (1990).
[9] A. R. Heyd, Ilsin An, R. W. Collins, Yue Cong, K. Vedam, S. S. Bose, and D. L. Miller, J. Vac. Sci. Technol. A **9**, 810 (1991).
[10] P. G. Snyder, M. C. Rost, G. H. Bu-Abbud, J. A. Woollam, and S. A. Alterovitz, J. Appl. Phys. **60**, 3293 (1986).
[11] R. Bhat, W. K. Chan, A. Kastalsky, M. A. Koza, and P. S. Davisson, Appl. Phys. Lett. **47**, 1344 (1985).
[12] S. Luryi and F. Capasso, Appl. Phys. Lett. **47**, 1347 (1985).
[13] F. L. Terry, Jr., J. Appl. Phys. **70**, 409 (1991).
[14] M. Erman, J. B. Theeten, P. Frijlink, S. Gaillard, Fan Jia Hia, and C. Alibert, J. Appl. Phys. **56**, 3241 (1984).
[15] P. G. Snyder, J. A. Woollam, and S. A. Alterovitz, Proc. MRS Symp. **77**, 761 (1987).
[16] P. G. Snyder, J. A. Woollam, S. A. Alterovitz, and B. Johs, J. Appl. Phys. **68**, 5925 (1990).
[17] S. Adachi, J. Appl. Phys. **58**, 1 (1985).
[18] S. Adachi, Phys. Rev. B **38**, 12345 (1988).
[19] D. W. Jenkins, J. Appl. Phys. **68**, 1848 (1990).
[20] J. R. Chelikowski and M. L. Cohen, Phys. Rev. B **14**, 556 (1976).
[21] P. Lautenschlager, M. Garriga, S. Logothetidis, and M. Cardona, Phys. Rev. B **35**, 9174 (1987).
[22] The spectral data (Ref. 6) for $x = 0.8$ and 0.9 have low peak values in the E_2 complex region due to poor sample quality, which arises from the high reactivity of the Al component in the atmosphere.
[23] J. W. Garland, C. C. Kim, H. Abad, and P. M. Raccah, Phys. Rev. B **41**, 7602 (1990).
[24] D. E. Aspnes, in *Handbook on Semiconductors*, edited by M. Balkanski (North-Holland, Amsterdam, 1980), Vol. 2, p. 109.
[25] M. Cardona, *Modulation Spectroscopy*, Supplement 11 of *Solid State Physics* (Academic, New York, 1969).
[26] S. Adachi, Phys. Rev. B **35**, 7454 (1987).
[27] The photon-energy range of $L(\omega_j, x_k)$ is from 1.5 and 6 eV, except $L(\omega_j, 0)$. The photon-energy range of $L(\omega_j, x_k)$ is from 1.0 to 6 eV in order to include E_0 of GaAs. The data preparation for $L(\omega_j, 0)$ is explained in the preceding paper (Ref. 1). The composition range of $L(\omega_j, x_k)$ is from 0 to 1,

but $L(\omega_j, 0.9)$ is not included in our fit since $L(\omega_j, 0.9)$ is not reliable. When Aspnes *et al.* (Ref. 6) reported $L(\omega_j, x_k)$, they suggested two sets of data for x_k. We choose to use the target compostion for x_k, instead of using the recalculated values for x_k. However, the procedures described in this paper are equally valid if one uses the recalculated values for x_k.

[28]O. Berolo and J. C. Woolley, Can. J. Phys. **49**, 1335 (1971).
[29]D. E. Aspnes, Surf. Sci. **135**, 284 (1983).
[30]S. Logothetidis, M. Alouani, M. Garriga, and M. Cardona, Phys. Rev. B **41**, 2959 (1990).
[31]A. Onton (unpublished).
[32]S. Adachi, J. Appl. Phys. **66**, 6030 (1989).
[33]H. C. Casey, D. D. Sell, and M. B. Panish, Appl. Phys. Lett. **24**, 63 (1974).
[34]R. E. Fern and A. Onton, J. Appl. Phys. **42**, 3499 (1971).
[35]M. A. Afromowitz, Solid State Commun. **15**, 59 (1974).
[36]H. Arwin and D. E. Aspnes, J. Vac. Sci. Technol. A **2**, 1316 (1984).
[37]L. Vina, C. Umbach, M. Cardona, and L. Vodopyanov, Phys. Rev. B **29**, 6752 (1984).
[38]S. M. Kelso, D. E. Aspnes, M. A. Pollack, and R. E. Nahory, Phys. Rev. B **26**, 6669 (1982).
[39]K. Kumazaki, L. Viña, C. Umbach, and M. Cardona, Phys. Status Solidi B **156**, 371 (1989).
[40]M. Erman, J. P. Andre, and J. Le Bris, J. Appl. Phys. **59**, 2019 (1986).
[41]B. Drevillon, E. Bertran, P. Alnot, J. Olivier, and M. Razeghi, J. Appl. Phys. **60**, 3512 (1986).
[42]S. Adachi, Phys. Rev. B **41**, 1003 (1990); P. S. Davisson, Appl. Phys. Lett. **47**, 1344 (1985).
[43]H. Yao, P. G. Snyder, and J. A. Woollam, J. Appl. Phys. **70**, 3261 (1991).